Superior self-powered room-temperature chemical sensing with light-activated inorganic halides perovskites

Hongjun Chen*, Meng Zhang, Renheng Bo, Chog Barugkin, Jianghui Zheng, Qingshan Ma, Shujuan Huang, Anita W. Y, Ho-Baillie, Kylie R. Catchpole and Antonio Tricoli*

H. Chen and M. Zhang make equal contribution

Dr. H. Chen, R. Bo, A/Prof. A. Tricloi

Nanotechnology Research Laboratory, Research School of Engineering, Australian National University, Canberra 2601, Australia
E-mail: antonio.tricoli@anu.edu.au; hongjun.chen@anu.edu.au

Dr. M. Zhang, J. Zheng, Q. Ma, Dr. S. Huang, Dr. A. W.Y. Ho-balillie
Australian Centre for Advanced Photovoltaics, School of Photovoltaic and Renewable Energy Engineering, University of New South Wales, Sydney 2052, Australia

Dr. C. Barugkin, Prof. K. R. Catchpole

Research School of Engineering, Australian National University, Canberra 2601, Australia

The hybrid halide perovskite is one of the promising light absorber and intensively investigated for many optoelectronic applications. Here, we present the first prototype of self-powered inorganic halides perovskite for chemical gas sensing at room temperature under visible-light irradiation. These devices consist of porous network of $CsPbBr_3$ (CPB) and can generate an open circuit voltage of 0.87 V under visible-light irradiation, which can be used to detect various concentrations of O_2 and per million concentrations of medically-relevant volatile organic compounds such as acetone and ethanol with very quick response and recovery time. It is observed that O_2 gas can passivate the surface trap sites in CPB and the ambipolar charge transport in the perovskite layer results in a distinct sensing mechanism than established semiconductors with symmetric electrical response to both oxidizing and reducing gases. The platform of CPB based gas sensor provides new insights for the emerging area of wearable sensors for personalized and preventive medicine.

The development of wearable devices for the personalized and continuous monitoring of important metabolic markers is driving a renaissance in solid-state sensor technologies.[1] In particular, analysis of the footprint of volatile organic compounds (VOCs) released through the human breath is a powerful approach for the contact-less monitoring and diagnostics of numerous diseases including diabetes,[2] asthma[3] and breast cancer.[1, 4] A major challenge for the wide spread utilization of these non-invasive medical technologies remains the engineering of miniaturized chemical sensors capable to measure trace-concentrations of multiple biomarkers in complex gas mixtures with low power consumption and on-chip integration potential.[5] The search for self-powered materials that responds to small variations in their chemical environment with a significant change in their electrical properties at room temperature is a game-changing aim with the potential to revolutionize future wearable sensor technologies.[1]

Solid-state chemical sensors, based on nanostructured metal oxide semiconductors, are amongst the smallest sensing technology that can be easily integrated in chip without the need of movable and optical components. Despite numerous advantages, the latter usually rely on relatively high

temperatures (200-500 °C)[6] and an external bias to activate the sensing reactions and signal transduction.[5, 7] Recently, UV light activation has been utilized to lower the required operation temperature facilitating the use of some wide bandgap semiconductors.[8] However, an external bias and generation of potentially harmful UV radiation is still required.[8] Very recently, silicon-based hybrid nanowire morphologies have been reported as a successful architecture for self-powered chemical sensing demonstrating detection of down to 0.27% of ethanol concentration in hexane at room-temperature.[7, 9, 10] In addition to achieving detection of volatile organic compounds in ppm-ppb concentration, future improvements are required to accelerate the relatively slow sensing kinetics,[7, 10] and simplify the laborious fabrication process[7, 9, 10] of these promising devices.

Featuring a tunable optical band gap,[11, 12] high carrier mobility and lifetime,[13] low exciton binding energy,[14] and a broad absorption range with high extinction coefficient,[15] organic-inorganic hybrid halide perovskites have generated enormous interest as one of the most promising emerging light absorbers for optoelectronic applications.[16-20] Recently, to alleviate the limited stability and environmental sensitivity of organic-inorganic hybrid halides perovskites, inorganic cations like Cs have been explored as a substitute for the organic cations.[11, 21-24] In particular, $CsPbBr_3$ (CPB) is a highly photoresponsive material[25] with excellent electron and hole mobility[25, 26] that has shown better stability[27, 28] and resilience to environmental degradation[29] than optoelectronic devices based on organic-inorganic hybrid halide perovskites.

Here, CPB inorganic perovskite was chosen due to its superior stablilty at ambient condition [27, 28] and we report the first use of inorganic halide perovskites for self-powered chemical sensing, demonstrating room-temperature detection of medically-relevant volatile organic compounds in

ppm concentrations. We investigate the electrical response of porous interconnected layers of $CsPbBr_3$ nanocrystals to small changes in their chemical environment with and without photo excitation. Our findings reveal that under visible light-activation, the photocurrent generated by these $CsPbBr_3$-based devices is highly sensitive to the concentration of oxidizing and reducing gas molecules. Surprisingly, the $CsPbBr_3$ sensing mechanism is distinct from that of nanostructured semiconductors showing a symmetrical electrical response to both oxidizing and reducing gases. These new insights on the photo-chemical properties of inorganic halides perovskites provide new exciting opportunities for the engineering of solid-state sensors with application including wearable medical devices and self-powered environmental monitoring.

Fig. 1 shows a schematic of the CPB sensor layout and its morphological, structural and optical characterizations. The device consists of a porous and interconnected layer of CPB crystals deposited on a fluorine-doped tin oxide layer (FTO). The electrical response of CPB layer to the change in the composition of its chemical environment is measured across its cross-section by contacting its top surface and the FTO layer. Electron microscope analysis reveals a well-adhering and homogenous CPB layer with an average thickness of 350 ± 5 nm over the FTO surface (Fig. 1b-d). Both top view and cross-sectional analysis confirm the successful synthesis of a porous open-layer morphology constituted of interconnected grains of 100-200 nm in diameter. Under higher magnification, the grains are arranged in densely packed regions with well-sintered interparticle necks that are separated by throughout holes exposing the FTO surface (Fig. 1c). This open-layer interconnected morphology is beneficial in exposing the CPB surface to the target gas molecules while providing a continuous path for the collection of the photo-excited charges.

Fig. 1e and f summarizes the structural and optical characterization of these devices. The X-ray diffraction patterns of the CPB/FTO are denoted by five peaks matching the (100), (110), (200), (201) and (202) crystal planes of the monoclinic structure of $CsPbBr_3$ (JCPDS: 18-0364) and corresponding to an average crystal size of 58 nm. The optical absorbance spectra and the corresponding Tauc plot of our nanocrystalline CPB match well those previously reported for CPB indicating an onset of the absorbance at ~ 545 nm[18a] and a room temperature bandgap of 2.33 eV[29] (Fig. 1f). The photoluminescence (PL) spectrum shows a strong emission peak at ~ 546 nm (2.27 eV),[23, 25] which is very close to its optical band edge. These results demonstrate the successful synthesis of an open-layer porous morphology made of nanocrystalline CPB and featuring excellent optical and structural properties for visible light absorption and transport of the generated electron-hole pairs.

Fig. 2 demonstrates the use of these CPB devices for the self-powered chemical sensing of O_2, a strong oxidizing gas, at room-temperature providing first insights of the photoexcited charge carriers (AM 1.5 > 420 nm). A typical current-voltage plot of the CPB devices is displayed in Fig. S1 showing an open-circuit voltage 0.87 V and a short-circuit current density of 1.94 nA/cm^2 at room temperature under visible light illumination (AM 1.5, > 420 nm). Although the power-generated by these devices is low if compared with CPB-based solar cells,[23, 27-29] this is due to their porous open-layer morphology featuring a non-passivated surface, and the lack of any blocking and top charge collection layers. Most importantly, the power generated by these first prototypes is sufficient to drive the sensing reactions and their electrical transduction providing a simple but effective demonstration of a self-powered perovskite chemical sensor. Notably, in dark, the devices have very small currents in the range of 0.1 pA (Fig. 2a, broken line) and do not show any measurable variation in dark-current when switching the atmosphere from pure N_2 to pure O_2. This

indicates none or very poor chemical sensitivity. In strong contrast, under visible light illumination, the photocurrent increases by ca. 4 orders of magnitude to ca. 1.5 nA. The illuminated devices respond to the O_2 atmosphere with a nearly 100% rise of the photocurrent to 2.57 nA (Fig. 2a, continuous line). Analysis of their response dynamics (Fig. 2b), show that the photocurrent increases rapidly and stabilizes upon O_2 injection, and quickly recovers to its initial value after switching back to the pure N_2 atmosphere. The CPB sensor responsivity ((I_{O2}-I_{N2})/I_{N2}) to exposure to pure O_2 is in the range of 0.93 with a swift response (t_{rs}) and recovery times (t_{rc}) of only 17 and 128 s, respectively. This is significantly faster than that (~1200 s) reported for self-powered Si-ZnO gas sensors,[7, 10] and outstanding even with respect to best performing room-temperature chemoresistive devices.[5] Fig. 2c shows four consecutive N_2/O_2 switching cycles revealing a good stability of the sensor response, and prompt recovery of the baseline photocurrents. A plot of the sensor responsivity versus the logarithmic concentration of O_2 from 100% to 1% in N_2 shows a linear dependency with a goodness of fit of 0.99 (Fig. 2d), and an excellent response range with no saturation up to ca. 100% O_2. The CPB devices could easily detect down to 1%, and possibly less concentrations, of O_2 in N_2, which is more than sufficient for application in medical O_2 sensors.

To further investigate the sensing mechanism of these photoexcited CPB layers, acetone and ethanol were chosen as exemplary reducing gases as they are important volatiles biomarkers related to diabetes[2] and non-invasive estimation of the blood glucose content from breath analysis.[30] Fig. 3a and b shows that the CPB devices can quickly detect acetone (Fig. 3a) and ethanol (Fig. 3b) concentrations as low as 1 ppm in simulated air with a sensor responsivity of ca. 0.03 and 0.025, respectively. The absolute values of the currents upon exposure to 1 ppm of ethanol and acetone were ca. 1.98 and 3.95 nA (Figure S4), respectively. This is an excellent performance with respect to

other self-powered devices,[7, 9, 10] and even in comparison to wide bandgap semiconductors operated at significantly higher temperatures (250 - 450 °C).[5] Notably, the CPB response and recovery times to acetone were 9.8 and 5.8 s, respectively, challenging the fastest metal oxide semiconductor-based (MOS) devices so far reported.[5] Fig. 3c shows that similarity to the liner relationship between the sensor sensitivity and O_2 concentration, these perovskites shows a similar linear electrical response to increasing the ethanol concentration from 1 to 8ppm. Fig. S3 shows the response of the CPB sensors to four consecutive exposures to 4 ppm of ethanol. Despite some noise due to the challenge of contacting the porous top perovskite surface, the sensor reveals a good repeatability of the sensor sensitivity. Fig. 3d shows the sensor sensitivity to 1 ppm of ethanol has a function of the illumination power density from 13.3 to 37.8 mW/cm^2. The maximal sensitivity of 0.025 is achieved at the highest illumination power density of 37.8 mW/cm^2. Decreasing the power density to 13.3 mW/cm^2 decreases the sensitivity by ca. 25%. Table 1 presents a comparative summary of the key figure of merits of these perovskite-based devices against state-of-the-art solid-state chemical sensors activated with visible light. These first CPB prototypes demonstrate the lowest limit of detection for acetone and ethanol with faster response demonstrated at room temperature. The latter is particularly surprising as usually adsorption and desorption process have significantly slower rates at room temperature resulting in recovery times of several minutes to hours. Here, it is suggested that the relatively large pore and grain size (100 - 500 nm) of the CPB increase the effective gas diffusion coefficients facilitating their penetration and evacuation. This morphology cannot be easily implemented with established MOS materials as they need grain sizes below their Debye lengths (ca. 6 - 30 nm) to achieve sufficiently strong electrical transduction of the gas reactions on their surfaces.[5] This small grain size leads to nano- and micro-pores of few

7

nanometers, and thus slow the sensor response and recovery times at room-temperature. Similarly to the interaction with O_2 (Fig. 2a), in dark the CPB had no response to acetone and ethanol. This further suggests that the visible-light excited charges within CPB are strongly related to its sensing mechanism. Surprisingly, the response to reducing analytes was also characterized by an increase in photocurrent as the response to the oxidizing analyte. This indicates a distinct gas sensing mechanism than that of established MOS technologies. It is reported that halide perovskites are ambipolar charge transporters because of the similarity of electron effective mass and hole effective mass.[17, 31-33] There is no orbital or electron contribution from the cation to the final electronic structure of lead halide perovskite, although the cation can still affect the electronic structure through the steric effect.[17] Recently, it is pointed out that the surface trap sites in the perovskite play an important role in determining the optoelectronic properties.[34-36] Meanwhile, it is also reported that a net positive charge formed at the perovskite surface due to the loss of bromide and undercoordination of the Pb atom at the surface, which causes the perovskite sensitive to the environmental gases. As a type of "molecular gating", O_2 can donate electron to the Pb^{2+} cation and neutralize the excess positive charges and therefore to drastically modulate the surface recombination rate in the perovskite, demonstrating strong PL emission with O_2 gas but weak PL emission at vacuum.[35] In agreement with these findings, CPB demonstrates reversible gas sensing response to O_2 in our research, indicating that the surface trap sites in CPB play a key role in this gas sensing process. When purged in acetone/ethanol gases, the photo-excited electrons and holes in CPB under visible-light illumination may directly involve in the oxidization reaction or through the mediation of absorbed O_2, which results in the decrease of the concentration of electrons/holes. This still contribute to an increase in photocurrent by decreasing electron-hole recombination and

allowing for more free charge carriers within CPB. Recently, it was observed that the MAPbI$_3$ perovskite demonstrate good gas sensing response to O$_2$ and it was proposed that the iodine anion vacancies in the perovskite play as the active sites for gas sensing process.[36] Here CPB demonstrate a similar gas sensing response to O$_2$. We propose that O$_2$, ethanol or acetone act as vacancy filler and reversibly fill in intrinsic bromine vacancies of the CPB. Since bromine vacancies act as traps for the photoexcited charges, once the CPB is exposed to the target analyte the density of bromine vacancies decreases and a higher number of photoexcited charges is available for electrical transport resulting in the observed increase in photocurrent with increasing concentration of O$_2$, ethanol or acetone. It should be noted that under visible-light excitation the photo-excited electrons in CPB will be transferred to FTO, while the photo-excited holes will transfer to Au probe due to different Fermi levels (Figure S2, b). Thus, there is a current flowing through the out circuit of the CPB devices without application of an external bias (Fig. S2, a). Further, more in depth-studies are required to confirm the underlying gas sensing mechanism of these halide perovskites.

Fig. 4 shows some insights on the mid-term stability of these CPB devices. It should be noted that the samples are normally stored in a vacuum desiccator except the sensing measurements and characterizations. Upon 2 weeks storage and testing, these CPB sensors maintained a strong similar response to O$_2$ exposure. The slight increase of sensor responsivity from ~0.94 for the fresh sample to ~1.2, after two weeks, might be related to some alteration of the CPB structure.[11, 21] The XRD analysis reveals that upon 2 weeks the device structure still closely matches the CPB monoclinic phase with the exception of a new peak appearing at 11.9°. However, while the absorbance spectrum of CPB/FTO shows no significant variation (Fig. 4c), the PL emission peak decreased in intensity by ~ 17.4 times suggesting some possible degradation. The measured PL decay is attributed

to the formation of impurity in CPB [39] as revealed by the new XRD peak located at 2θ of 11.9° after 2 weeks (Fig. 4b). The stability of perovskites, and in particular their sensitivity to moisture, is a known issue for several applications including solar cells, diodes, photodectors and gas sensors. Despite this relatively poor stability of these type of perovskites, the CPB perovskite is a pure inorganic perovskite and more stable than most other organic-inorganic hybrid perovskites.[10, 27, 28] We have observed that the device can last for more than 7 hours under gas sensing and visible-light irradiation and demonstrate good reproducibility of the sensing properties after 2 weeks storage (Figure 4). Investigation and possibly improvement of the long-term material stability may be required for their future integration in commercial devices.

Fabrication of the hybrid perovskite films on flexible substrate has been recently demonstrated. [37, 38] Here, the low synthesis and operation temperatures of these perovskite sensing layers of 100 and 30 ^{o}C, respectively, will facilitate their future fabrication on flexible substrates. As for most chemo-resistive gas sensors the selectivity is an issue.[5] For these type of devices, the most common ways to increase the selectivity is to use membranes, which can enable the permeation of selected gases, or the integration of multiple sensors with pattern recognition approaches that are able to determine both the concentration and type of gas in relatively complex gas mixtures.[1] Despite the toxicity of lead-based perovskite materials, considering the small size of the sensing surface required (100 μm^2),[47] these devices can be integrated in wearable devices where water-proof membrane can be implemented.

Overall, these inorganic halide perovskites are a new promising member of the chemical-sensing materials family providing some distinctive and appealing features, not found in established metal oxide semiconductor technologies. The lowest concentration of volatile organic compounds

(acetone and ethanol) and O_2 measured were 1 ppm and 10000 ppm, respectively. Notably, the photoexcited charge carriers in the $CsPbBr_3$ play a dual role in chemical sensing and power generation. The ambipolar charge transport in the $CsPbBr_3$ gives rise to a distinct room-temperature sensing mechanism that overcomes some of the limitations of state-of-the-art semiconductors. These self-powered $CsPbBr_3$ prototypes demonstrate already exemplary sensing of important volatile metabolic markers such as one particle per million of acetone at room temperature with fast response and recovery times. We believe that these exciting insights on the chemical response of photoexcited $CsPbBr_3$ provide new directions for the design of room-temperature and self-powered chemical sensors with application extending from personalized healthcare monitoring to public space safety. However, there are numerous challenges that need to be addressed to achieve commercial perovskite chemical sensors in the future. Moisture-resistive perovskite or water-protective layers with can selective allow permeation of the target analyte needs to be developed to improve long-term stability. Engineering of non-lead perovskites and their deposition on flexible substrates is important for their integration on wearable electronic devices. Tuning composition of the perovskites is a promising direction to tune the selectivity of these self-powered devices to specific target analytes.

Experimental Section

Synthesis of CsPbBr₃ film: The gas sensor device was fabricated by spin-coating of $CsPbBr_3$ film on FTO glass. The pre-etched FTO glass (Pilkington, 7 Ω cm-1) was cleaned with soap water, acetone, 2-propanol sequentially and then transferred to a UVO cleaner for a 20 min of UVO cleaning. The precursor solution of $CsPbBr_3$ was prepared by dissolving 0.5 M CsBr (Alfa Aesar) and 0.5 M $PbBr_2$ (Alfa Aesar) in Dimethyl sulfoxide (DMSO, Sigma-Aldrich). For spin-coating of $CsPbBr_3$ film, 20 µL of

precursor solution was dispensed on cleaned FTO substrate and then spun at 3000 rpm for 40 s. After spinning, the sample was put on a hot plate set at 100 ^{o}C for 15 min's of annealing.

Gas sensing measurement and characterization: The sensor measurements were performed as follow. For gas sensing of O_2, O_2 (BOC gas) and N_2 (BOC gas) were controlled by mass flow controller (Bronkhorst) but keep the total gas flow rate of 0.5 L/min. While ethanol (9.91 ppm in N_2, Coregas) and acetone (10 ppm in N_2, Coregas) were diluted to 1 ppm with simulated air (0.1 L/min O_2 + 0.4 L/min N_2, BOC) before purging into the chamber and the total flow rate is still 0.5 L/min. The temperature of the hotplate in a chamber (Linkam) was controlled by a temperature controller and the sample was illuminated through a quartz window by a solar simulator (NewSpec, LCS-100) with an AM1.5 filter glass and a 420 nm long pass glass filter (> 420 nm, Thorlabs Inc). For the gas sensing measurements, two gold probes were separately placed on top of the bare FTO and the CPB film under short-circuit condition and the dynamic response of gas sensor was recorded by an electrochemical workstation (CHI 660E, USA). The electrode surface is ca. 0.5 cm^{-2} and the irradiation power is 37.8 mW/cm^2 (Table 1). The Jsc and Voc were obtained through I-V scan from 0 to 1 V of FTO/CsPbBr$_3$ device under visible-light irradiation or in dark condition.

The morphology was investigated by using Zeiss Ultraplus (FESEM) at 3 kV. A micro-photoluminescence spectroscopy was used to collect the steady-state-photoluminescence spectra at room temperature. A linearly polarized pulsed laser (frequency doubled to 522 nm with 300 fs pulse width and 20.8 MHz repetition rate) is directed through a 10X objective lens to excite the sample and the emitted PL signal is collected by a monochromators and a charge coupled device (CCD) (Princeton Instruments, PIXIS). The average excitation power of the laser is 1μW on the sample. The crystalinity was characterized by X-ray diffraction using Bruker system (XRD, D 2 Phaser, USA)

equipped with Cu Kα radiation of average wavelength 1.54059 Å. The absorbance spectra were measured with a Perkin–Elmer (Lambda 1050 UV/vis/NIR) Spectrophotometer and a 150 mm integrating sphere.

Supporting Information

Supporting Information is available from the Wiley Online Library or from the author.

Received: ((will be filled in by the editorial staff))
Revised: ((will be filled in by the editorial staff))
Published online: ((will be filled in by the editorial staff))

WILEY-VCH

Author Manuscript

14

References

1. Tricoli, A.; Nasiri, N.; De, S., *Adv. Funct. Mater.* **2017,** *27*, DOI: 10.1002/adfm.201605271.
2. Marco, R.; Antonio, T., *J. Breath. Res.* **2011,** *5*, 037109.
3. Smith , A. D.; Cowan , J. O.; Brassett , K. P.; Herbison , G. P.; Taylor , D. R., *N. Engl. J. Med.* **2005,** *352*, 2163-2173.
4. Barash, O.; Zhang, W.; Halpern, J. M.; Hua, Q.-L.; Pan, Y.-Y.; Kayal, H.; Khoury, K.; Liu, H.; Davies, M. P. A.; Haick, H., *Oncotarget* **2015,** *6*, 44864-44876.
5. Tricoli, A.; Righettoni, M.; Teleki, A., *Angew. Chem. Int. Ed.* **2010,** *49*, 7632-7659.
6. Zhou, X.; Lee, S.; Xu, Z.; Yoon, J., *Chem. Rev.* **2015,** *115*, 7944-8000.
7. Hoffmann, M. W. G.; Mayrhofer, L.; Casals, O.; Caccamo, L.; Hernandez-Ramirez, F.; Lilienkamp, G.; Daum, W.; Moseler, M.; Waag, A.; Shen, H.; Prades, J. D., *Adv. Mater.* **2014,** *26*, 8017-8022.
8. Zhang, J.; Liu, X.; Neri, G.; Pinna, N., *Adv. Mater.* **2016,** *28*, 795-831.
9. Wang, X.; Wang, Y.; Åberg, D.; Erhart, P.; Misra, N.; Noy, A.; Hamza, A. V.; Yang, J., *Adv. Mater.* **2011,** *23*, 117-121.
10. Hoffmann, M. W. G.; Gad, A. E.; Prades, J. D.; Hernandez-Ramirez, F.; Fiz, R.; Shen, H.; Mathur, S., *Nano Energy* **2013,** *2*, 514-522.
11. Sutton, R. J.; Eperon, G. E.; Miranda, L.; Parrott, E. S.; Kamino, B. A.; Patel, J. B.; Hörantner, M. T.; Johnston, M. B.; Haghighirad, A. A.; Moore, D. T.; Snaith, H. J., *Adv. Energy Mater.* **2016,** *6*, 10.1002/aenm.201502458.
12. Stranks, S. D.; Snaith, H. J., *Nat. Nano.* **2015,** *10*, 391-402.
13. Wehrenfennig, C.; Eperon, G. E.; Johnston, M. B.; Snaith, H. J.; Herz, L. M., *Adv. Mater.* **2014,** *26*, 1584-1589.
14. Miyata, A.; Mitioglu, A.; Plochocka, P.; Portugall, O.; Wang, J. T.-W.; Stranks, S. D.; Snaith, H. J.; Nicholas, R. J., *Nat. Phys.* **2015,** *11*, 582-587.
15. Barugkin, C.; Cong, J.; Duong, T.; Rahman, S.; Nguyen, H. T.; Macdonald, D.; White, T. P.; Catchpole, K. R., *J Phys. Chem. Lett.* **2015,** *6*, 767-772.
16. Zhang, M.; Yun, J. S.; Ma, Q.; Zheng, J.; Lau, C. F. J.; Deng, X.; Kim, J.; Kim, D.; Seidel, J.; Green, M. A.; Huang, S.; Ho-Baillie, A. W. Y., *ACS Energy Lett.* **2017,** *2*, 438-444.
17. Zhao, Y.; Zhu, K., *Chem. Soc. Rev.* **2016,** *45*, 655-689.
18. Chueh, C.-C.; Li, C.-Z.; Jen, A. K. Y., *Energy Environ. Sci.* **2015,** *8*, 1160-1189.
19. Li, M.-H.; Shen, P.-S.; Wang, K.-C.; Guo, T.-F.; Chen, P., *J. Mater. Chem. A* **2015,** *3*, 9011-9019.
20. Da, P.; Zheng, G., *Nano Research* **2017,** *10*, 1471-1497.
21. Ma, Q.; Huang, S.; Wen, X.; Green, M. A.; Ho-Baillie, A. W. Y., *Adv. Energy Mater.* **2016,** *6*, DOI: 10.1002/aenm.201502202.

22. Saliba, M.; Matsui, T.; Seo, J.-Y.; Domanski, K.; Correa-Baena, J.-P.; Nazeeruddin, M. K.; Zakeeruddin, S. M.; Tress, W.; Abate, A.; Hagfeldt, A.; Gratzel, M., *Energy Environ. Sci.* **2016,** *9*, 1989-1997.

23. Kulbak, M.; Cahen, D.; Hodes, G., *J Phys. Chem. Lett.* **2015,** *6*, 2452-2456.

24. McMeekin, D. P.; Sadoughi, G.; Rehman, W.; Eperon, G. E.; Saliba, M.; Hörantner, M. T.; Haghighirad, A.; Sakai, N.; Korte, L.; Rech, B.; Johnston, M. B.; Herz, L. M.; Snaith, H. J., *Science* **2016,** *351*, 151-155.

25. Stoumpos, C. C.; Malliakas, C. D.; Peters, J. A.; Liu, Z.; Sebastian, M.; Im, J.; Chasapis, T. C.; Wibowo, A. C.; Chung, D. Y.; Freeman, A. J.; Wessels, B. W.; Kanatzidis, M. G., *Cryst. Growth Des.* **2013,** *13*, 2722-2727.

26. Yettapu, G. R.; Talukdar, D.; Sarkar, S.; Swarnkar, A.; Nag, A.; Ghosh, P.; Mandal, P., *Nano Lett.* **2016,** *16*, 4838-4848.

27. Liang, J.; Wang, C.; Wang, Y.; Xu, Z.; Lu, Z.; Ma, Y.; Zhu, H.; Hu, Y.; Xiao, C.; Yi, X.; Zhu, G.; Lv, H.; Ma, L.; Chen, T.; Tie, Z.; Jin, Z.; Liu, J., *J Am. Chem. Soc.* **2016,** *138*, 15829-15832.

28. Beal, R. E.; Slotcavage, D. J.; Leijtens, T.; Bowring, A. R.; Belisle, R. A.; Nguyen, W. H.; Burkhard, G. F.; Hoke, E. T.; McGehee, M. D., *J Phys. Chem. Lett.* **2016,** *7*, 746-751.

29. Kulbak, M.; Gupta, S.; Kedem, N.; Levine, I.; Bendikov, T.; Hodes, G.; Cahen, D., *J Phys. Chem. Lett.* **2016,** *7*, 167-172.

30. Minh, T. D. C.; Oliver, S. R.; Ngo, J.; Flores, R.; Midyett, J.; Meinardi, S.; Carlson, M. K.; Rowland, F. S.; Blake, D. R.; Galassetti, P. R., *Am. J. Physiol. Endocrinol. Metab.* **2011,** *300*, E1166-E1175.

31. Ball, J. M.; Lee, M. M.; Hey, A.; Snaith, H. J., *Energy Environ. Sci.* **2013,** *6*, 1739-1743.

32. Giorgi, G.; Fujisawa, J.-I.; Segawa, H.; Yamashita, K., *J Phys. Chem. C* **2014,** *118*, 12176-12183.

33. Zhuang, Y.; Yuan, W.; Qian, L.; Chen, S.; Shi, G., *Phys. Chem. Chem. Phys.* **2017**, DOI: 10.1039/C7CP01646H.

34. Noel, N. K.; Abate, A.; Stranks, S. D.; Parrott, E. S.; Burlakov, V. M.; Goriely, A.; Snaith, H. J., *ACS Nano* **2014,** *8*, 9815-9821.

35. Fang, H.-H.; Adjokatse, S.; Wei, H.; Yang, J.; Blake, G. R.; Huang, J.; Even, J.; Loi, M. A., *Science Advances* **2016,** *2* (7). DOI 10.1126/sciadv.1600534.

36. Stoeckel, M.-A.; Gobbi, M.; Bonacchi, S.; Liscio, F.; Ferlauto, L.; Orgiu, E.; Samorì, P., *Adv. Mater.* **2017,** *29* (38), n/a-n/a. DOI 10.1002/adma.201702469.

37. Xu, X.; Chen, Q.; Hong, Z.; Zhou, H.; Liu, Z.; Chang, W.-H.; Sun, P.; Chen, H.; Marco, N. D.; Wang, M.; Yang, Y., *Nano Lett.* **2015,** *15*, 6514-6520.

38. Docampo, P.; Ball, J. M.; Darwich, M.; Eperon, G. E.; Snaith, H. J., *Nature Commun.* **2013,** *4*, 2761.

39. Pathak, S.; Sepe, A.; Sadhanala, A.; Deschler, F.; Haghighirad, A.; Sakai, N.; Goedel, K. C.; Stranks, S. D.; Noel, N.; Price, M.; Hüttner, S.; Hawkins, N. A.; Friend, R. H.; Steiner, U.; Snaith, H. J., *ACS Nano* **2015,** *9*, 2311-2320.

40. Geng, Q.; He, Z.; Chen, X.; Dai, W.; Wang, X., *Sens. Actuators B* **2013,** *188*, 293-297.

41. Peng, L.; Zeng, Q.; Song, H.; Qin, P.; Lei, M.; Tie, B.; Wang, T., *Appl. Phys. A* **2011,** *105*, 387-392.

42. Zhang, Y.; Liu, B.; Wang, D.; Lin, Y.; Xie, T.; Zhai, J., *Mater. Chem. Phys.* **2012,** *133*, 834-838.

43. Sivalingam, Y.; Martinelli, E.; Catini, A.; Magna, G.; Pomarico, G.; Basoli, F.; Paolesse, R.; Di Natale, C., *J Phys. Chem. C* **2012,** *116*, 9151-9157.

44. Zhang, P.; Pan, G.; Zhang, B.; Zhen, J.; Sun, Y., *Mat. Res.* **2014,** *17*, 817-822.

45. Wu, B.; Lin, Z.; Sheng, M.; Hou, S.; Xu, J., *Appl. Surf. Sci.* **2016,** *360*, 652-657.

46. Lin, Z.; Liao, F.; Zhu, L.; Lu, S.; Sheng, M.; Gao, S.; Shao, M., *CrystEngComm* **2014,** *16*, 4231-4235.

47. Tricoli, A.; Graf, M.; Mayer, F.; Kühne, S.; Hierlemann, A.; Pratsinis, S. E., Adv. Mater. 2008, 20, 3005-3010.
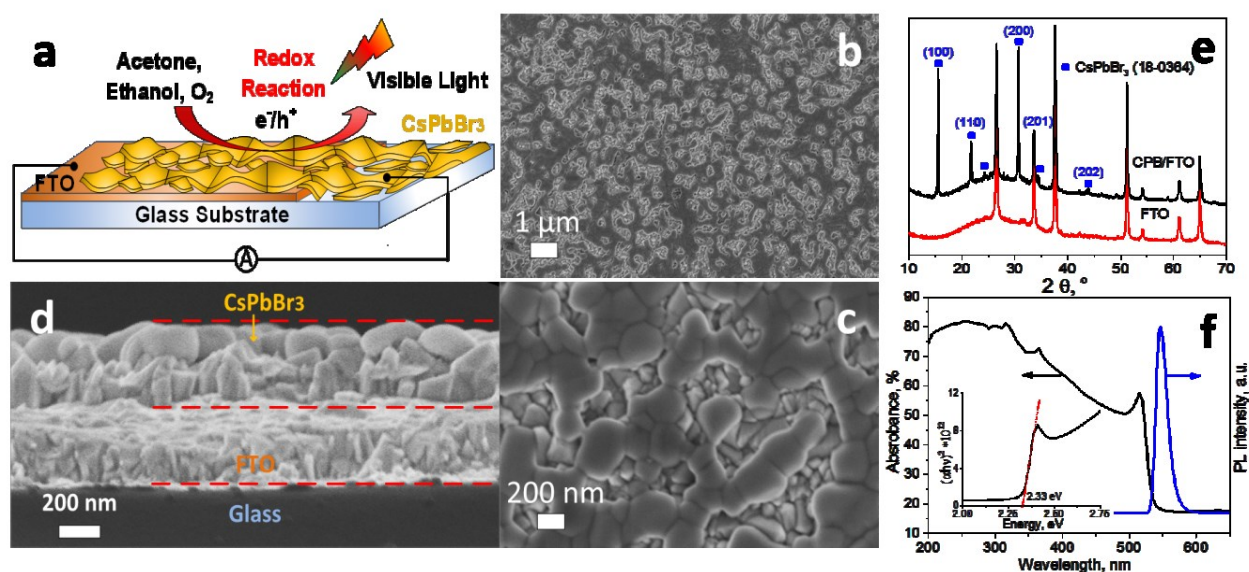
Figure 1. Schematic illustration of a CPB based chemical sensor and morphological, structural and optical characterizations. a, Schematic of O2 gas sensing by the CPB device. b,c,d, SEM images of an exemplary CPB films deposited on a FTO glass substrate showing its top view at low magnification (b) and high magnification (c), and its cross-section (d). e, XRD patterns of the CPB layers on the FTO (black line) and FTO reference (red line). f, Optical absorbance (black line) and PL spectra (blue line) of the CPB layers on the FTO and corresponding Trauc plot (inset).
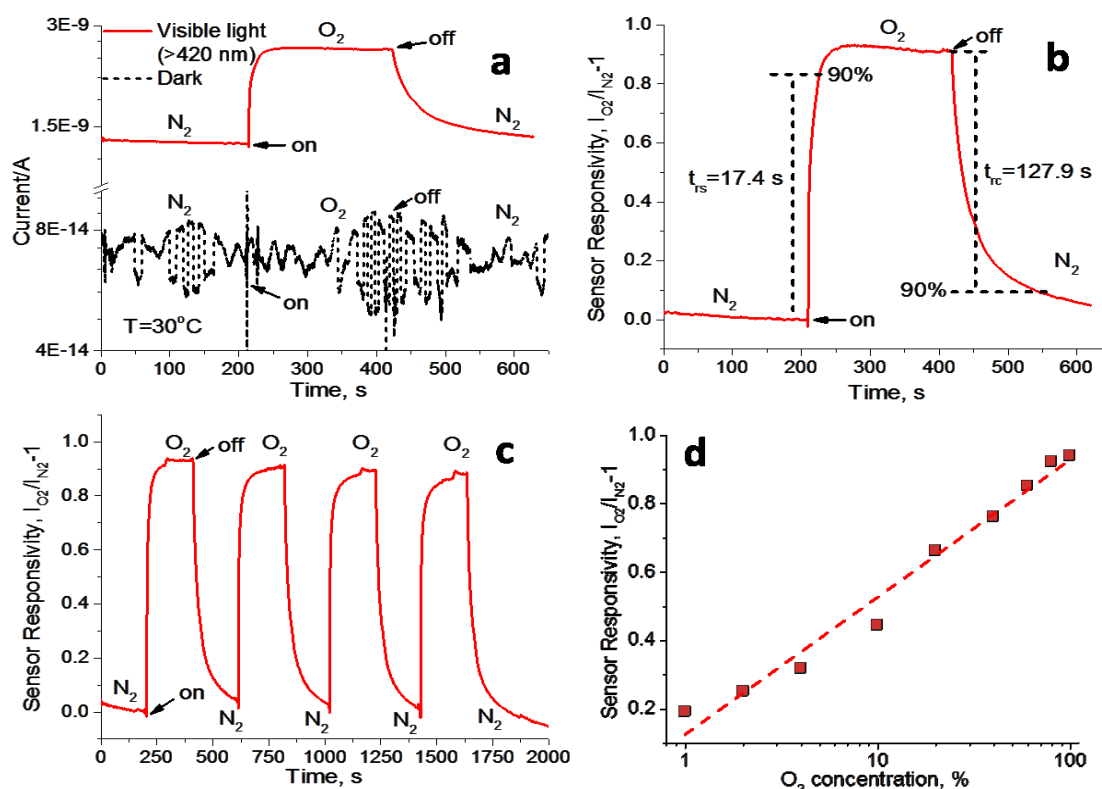
Figure 2. Characterization of the room-temperature chemical response of the CPB devices to an oxidizing gas under visible-light activation (AM 1.5, > 420 nm) and in dark conditions. a, Dynamic responses of a typical CPB sensor to switching the chemical environment from pure N_2 to pure O_2 in dark (broken line) and under visible-light illumination (red line). b, CPB sensor responsivity to the pure O_2 atmosphere under visible-light irradiation revealing a response (trs) and recovery (trc) time of 17.4 and 127.9 s, respectively. c, Stability of the CPB gas sensor response to the pure N2/O2 atmosphere switching under four consecutive cycles under visible-light illumination. d, CPB sensor responsivity as function of the O_2 concentration in N_2 from 1% to 100% under visible-light irradiation. The total flow rate was kept constant at 0.5 L/min for all experiments.
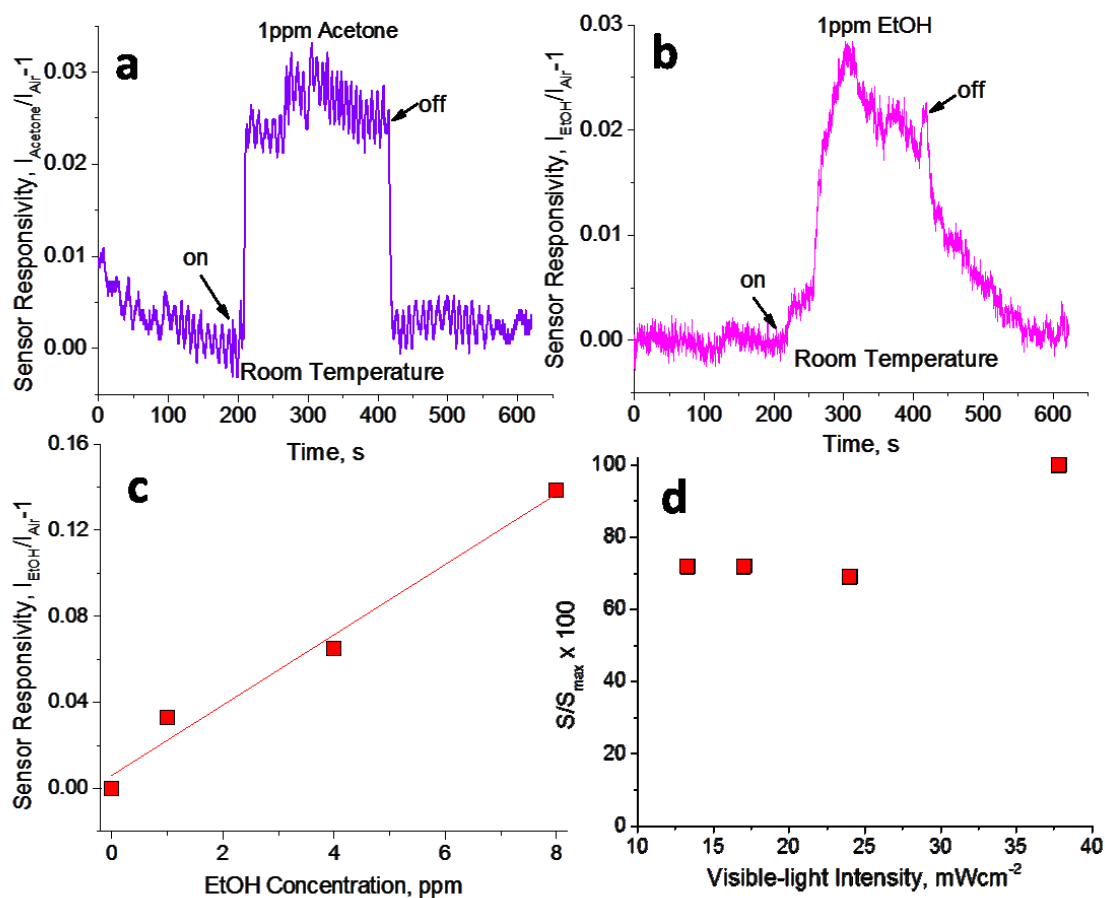
Figure 3. Characterization of the room-temperature chemical response of the CPB devices to two reducing gases under visible-light activation (AM 1.5, > 420 nm). Acetone and ethanol have been utilized as exemplary volatile organic compounds with relevance in non-invasive medical diagnostics. Dynamic CPB sensor responsivity to injection of 1 ppm of (a) acetone and (b) ethanol in air at room temperature under visible-light irradiation. Sensitivity of a photo-excited CPB devices a function of the sensitivity with the ethanol concentration from 1 to 8 ppm. (c) Sensor sensitivity to 1 ppm of ethanol has a function of the illumination power density from 13.3 to 37.8 mW/cm^2 (d). The gas sensing measurements were conducted under simulated air with a constant total gas flow of 0.5 L/min.
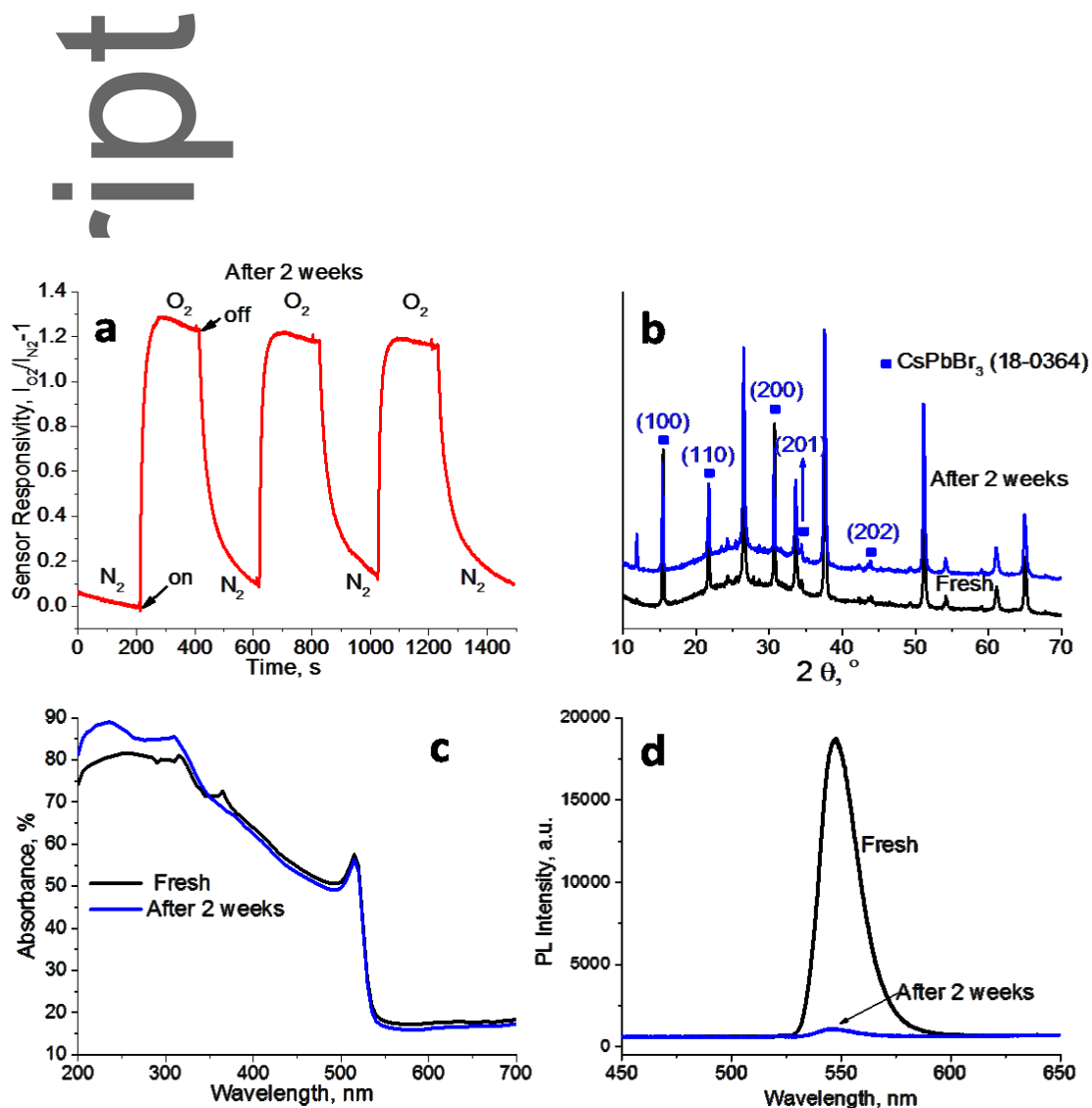
Figure 4. Characterization of the mid-term CPB sensor and material structure after 2 weeks of testing and storage. a, Three consecutive dynamic responses of the CPB sensor to a pure N2/O2 atmosphere switch at room temperature under visible-light irradiation (AM 1.5, > 420 nm). b,c,d, XRD patterns (b), absorbance (c) and PL (d) spectra of the CPB devices before (black lines) and after 2 weeks (blue lines).

21

WILEY-VCH

Table 1. Comparative summary of the key figure of merits of visible light-activated solid-state chemical sensors for sensing of volatile organic compounds (VOCs).

Material	Temperature	Light	Applied	Sensor	LOD[a]	Response/Recovery	Ref.

22

|	(^{o}C)	Intensity (mWcm^{-2})	Voltage (V)	Responsivity (I_{VOC}/I_{air}-1) (ppm-VOC)	(ppm)	Time (s)	
Porous CPB Network	30	37.8	0, Self-powered	0.03 (1 - Acetone) 0.025 (1 - EtOH)	1 1	ca. 10 / ca. 6 77/122	This work
ZnO film	RT[b]	ca. 1.49	8.5	~0.07 (700 - Acetone)	700	ca. 480 / 240	[40]
Cobalt-doped ZnO (1%) nanobelts	RT[b]	NM[c]	9.65	0.82 (ca. 13.8 – EtOH)	ca. 13.8	ca. 90/ ca. 1200	[41]
ZnO/Ag$_2$S microspheres	RT[b]	2	9.65	~0.11 (50 - EtOH)	50	<10	[42]
porphyrin-ZnO nanorods	30	NM[c]	1	~0.0067 (80 x10^3 - EtOH)	80 x10^3	N/A	[43]
7at% Sn-doped ZnO	65	NM[c]	5	399 (1000 - EtOH)	1000	1 / 5	[44]
ZnO/CdSe heterostructures	160	ca. 12.18	5	7.5 (25 - EtOH)	25	N/A	[45]
CdSe Nanoribbons	200	ca. 12.18	5	1.1 (50 - EtOH)	28	N/A	[46]

[a] Limit of detection; [b] room temperature, ca. 25°C; [c] not mentioned

The first prototype of self-powered inorganic halides perovskite is demonstrated for chemical gas sensing at room temperature under visible-light irradiation. These devices consist of porous network of $CsPbBr_3$ and can generate an open circuit voltage of 0.87 V under visible-light irradiation, which can be used to detect various concentrations of O_2 and per million concentrations of medically-relevant volatile organic compounds such as acetone and ethanol with very quick response and recovery time.

Keyword: *Inorganic halides perovskites; chemical gas sensors; self-powered; visible light, room temperature*

Hongjun Chen*, Meng Zhang, Renheng Bo, Chog Barugkin, Jianghui Zheng, Qingshan Ma, Shujuan Huang, Anita W. Y, Ho-Baillie, Kylie R. Catchpole and Antonio Tricoli*

Title: Superior self-powered room-temperature chemical sensing with light-activated inorganic halides perovskites
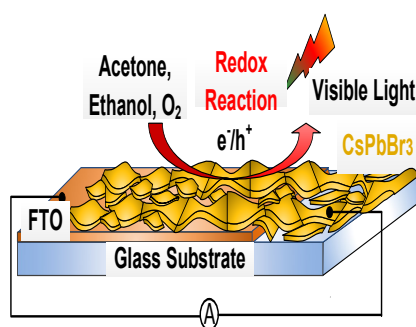
Supporting Information

Superior self-powered room-temperature chemical sensing with light-activated inorganic halides perovskites

Hongjun Chen*[#], Meng Zhang[#], Renheng Bo, Chog Barugkin, Jianghui Zheng, Qingshan Ma, Shujuan Huang, Anita W. Y, Ho-Baillie, Kylie R. Catchpole and Antonio Tricoli*
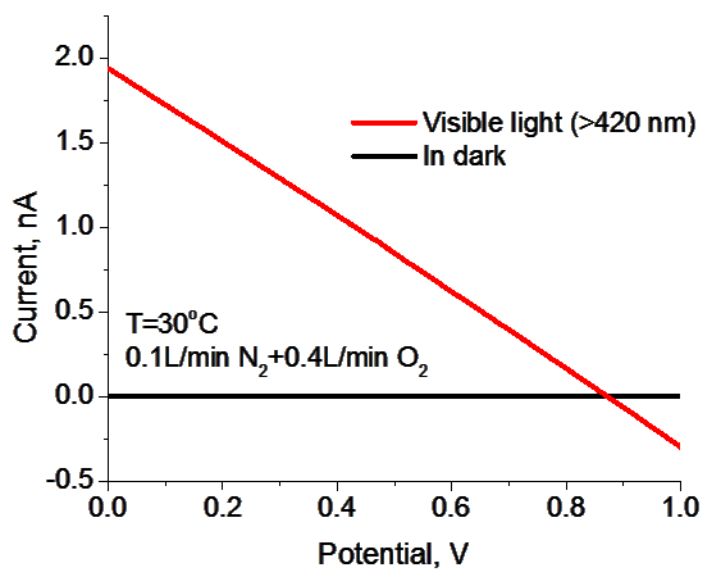
Figure S1. Current-voltage (I-V) plots of CPB/FTO based gas sensor under visible light (>420 nm) or in dark.
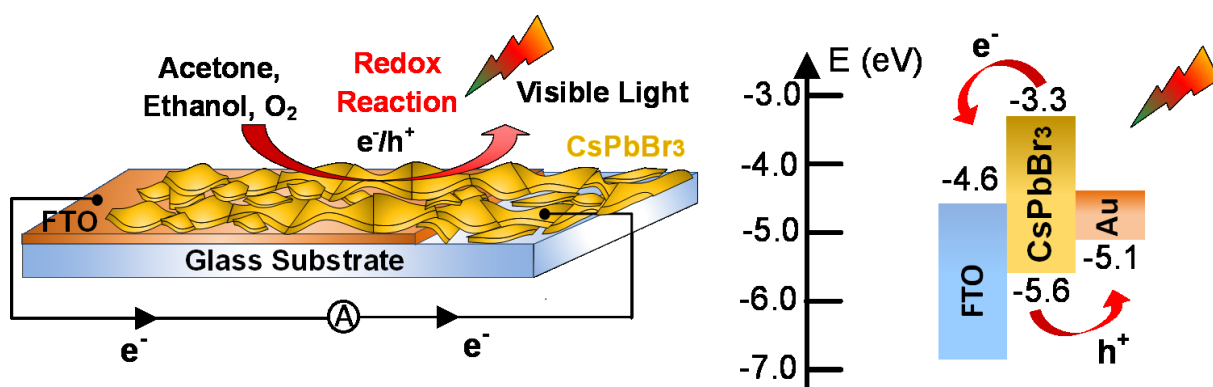
Figure S2. Scheme representation of the self-powered photocurrent flow in the CPB device (a) and the band diagram showing the photoexcited charges transfer process (b).
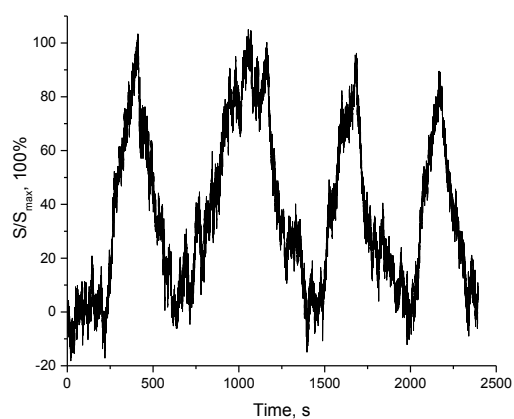
Figure S3. Response of the photo-excited CPB sensors to four consecutive exposures to 4 ppm of ethanol gas in air.
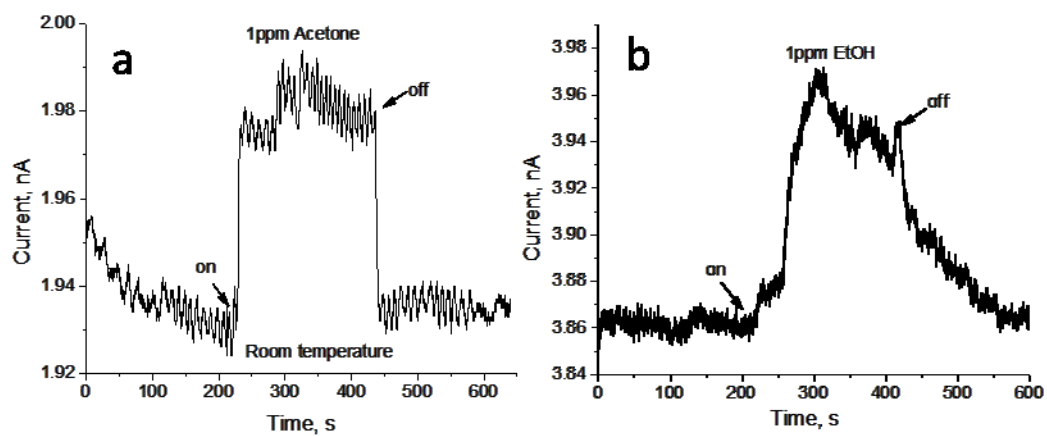
28

WILEY-VCH

Author Manuscript

29

Figure S4 Dynamic CPB sensor with absolute values of the current to injection of 1 ppm of (a) acetone and (b) ethanol in air at room temperature under visible-light irradiation.